photonics

MDPI

Communication

Holographic Writing of Forked Diffraction Gratings on the Surface of a Chalcogenide Glass Semiconductor

Nikolay A. Ivliev [1,2], Svetlana N. Khonina [1,2], Vladimir V. Podlipnov [1,2] and Sergey V. Karpeev [1,2,*]

[1] IPSI RAS-Branch of the FSRC Crystallography and Photonics RAS, 443001 Samara, Russia
[2] Samara National Research University, 443086 Samara, Russia
* Correspondence: karp@ipsiras.ru

Abstract: We consider the formation of forked diffraction gratings on the surface of a multilayer structure based on chalcogenide glass semiconductors As_2S_3 and a-Se is. The distribution of electric field components upon interference of beams with different polarization states is analyzed theoretically. The possibility of direct holographic writing of diffraction gratings with a "forked" structure is demonstrated. The parameters of vortex laser beams generated by the microrelief formed are examined.

Keywords: chalcogenide glass semiconductors; vortex laser beams; Mach–Zehnder interferometer

1. Introduction

Vortex laser beams [1–3] are currently attracting considerable attention of researchers due to a wide use of these beams in problems of atmospheric communication [4–8] and optical manipulation [9–11]. Vortex beams can be generated using a spatial light modulator (SLM) [12–14], anisotropic crystals [15–18], diffractive optical elements (DOEs) [19–24], metasurfaces [25–30], and various microelements [31,32]. Beams with a given phase distribution are most efficiently formed using DOEs; however, their production is a complex and expensive technological process.

One of the solutions to this problem is the use of anisotropic materials (for example, azobenzene-containing polymers (azopolymers)) that are sensitive to the orientation of the illuminating light polarization. Porfirev et al. [33,34] developed a technology for fabricating microstructures with specified profiles in azopolymer thin films patterned using structured light beams. Possibilities of producing helical microstructures [33], as well as various specified combinations of microprotrusions [34], were shown. The obtained relationship between the longitudinal component of the illuminating beam and the profile of the microstructure formed in a thin film allows the polarization state of the light to be used (both uniform and nonuniform) and information encoding/decoding based on this approach be implemented [34]. The authors of papers [35,36] presented a method of polarization holographic writing of forked diffraction gratings on the surface of films of a poly-N-epoxypropyl-carbazole copolymer and 4-(4-nitrophenyl azo)-aniline chromophore. The resulting surface structures make it possible to form vortex laser beams; however, the writing time at which the maximum diffraction efficiency of 24% is reached is 12 min.

Papers [37–39] present various methods for direct holographic writing of microreliefs on diffraction gratings in polarization-sensitive multilayer structures based on chalcogenide glass semiconductors As_2S_3 and a-Se, prepared by cyclic thermal vacuum evaporation of two materials from two isolated boats onto a constantly rotated glass substrate [39]. This technology makes it possible to obtain a more uniform application of nano multilayer coating and more homogeneous layers, unlike holographic coatings based on polymers. At the same time, chalcogenide materials have a high refractive index and can be effective in creating optical holographic metastructures. The diffraction efficiency of the formed gratings described in [38] reached 34% at a writing time of 5 min. This result was achieved

check for updates

Citation: Ivliev, N.A.; Khonina, S.N.; Podlipnov, V.V.; Karpeev, S.V. Holographic Writing of Forked Diffraction Gratings on the Surface of a Chalcogenide Glass Semiconductor. *Photonics* **2023**, *10*, 125. https://doi.org/10.3390/photonics10020125

Received: 21 December 2022
Revised: 14 January 2023
Accepted: 20 January 2023
Published: 27 January 2023

with the interference of linearly polarized beams incident at polarization angles of +45° and −45°. Moreover, a focusing system was used to increase the power density of the incident light. However, the mechanisms of influence of the polarization state of interfering beams on the writing process were not studied in the work.

In this paper, we consider the process of forming forked diffraction gratings in a multilayer structure based on chalcogenide glass semiconductors using a focusing system. It is known that such gratings are effectively used to generate and detect vortex beams [1–3]. The distribution of electric field components upon interference of beams with different polarization states is analyzed theoretically. The parameters of vortex laser beams formed by diffraction of the light on the formed microstructures are studied.

2. Theoretical Analysis

Holographic writing of linear diffraction gratings for various states of incident light polarization was studied by Achimova et al. [37] and Meshalkin et al. [40]. The experiments showed that the diffraction efficiency of the fabricated elements has a maximum value when one beam is linearly polarized at an angle of +45°, and the other is linearly polarized at an angle of −45°. Upon interference of P- and S-polarized beams, as well as of beams with left- and right-hand circular polarizations, the diffraction efficiency of surface structures is approximately the same and is two times lower than the maximum value. We analyze the interaction processes by simulating the distributions of various components of the electric field upon interference of differently polarized Gaussian beams. A Gaussian beam with a diameter σ in Cartesian coordinates (x, y) is described by the expression:

$$G(x,y) = \exp\left(-\frac{x^2+y^2}{\sigma^2}\right) \quad (1)$$

In our simulation, we consider a situation when two Gaussian beams are shifted relative to each other along the x axis in the input plane. The distributions of the total intensity in the focal plane and the distributions of the intensity of individual electric field components of the studied laser beams were calculated using the Richards–Wolf expressions [41,42]. Figure 1 presents the calculation results, and Figure 2 shows the intensity cross sections for the corresponding components of the focused field.

Input field	Electric field components			
	$\lvert\mathbf{E}\rvert^2$	$\lvert E_x\rvert^2$	$\lvert E_y\rvert^2$	$\lvert E_z\rvert^2$
a 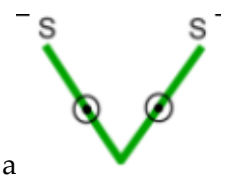	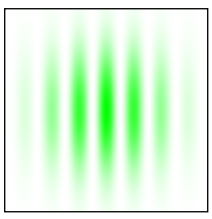	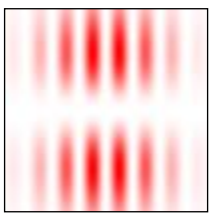	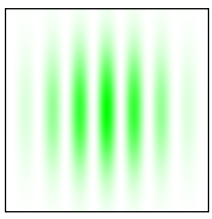	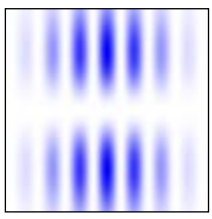

Figure 1. *Cont.*

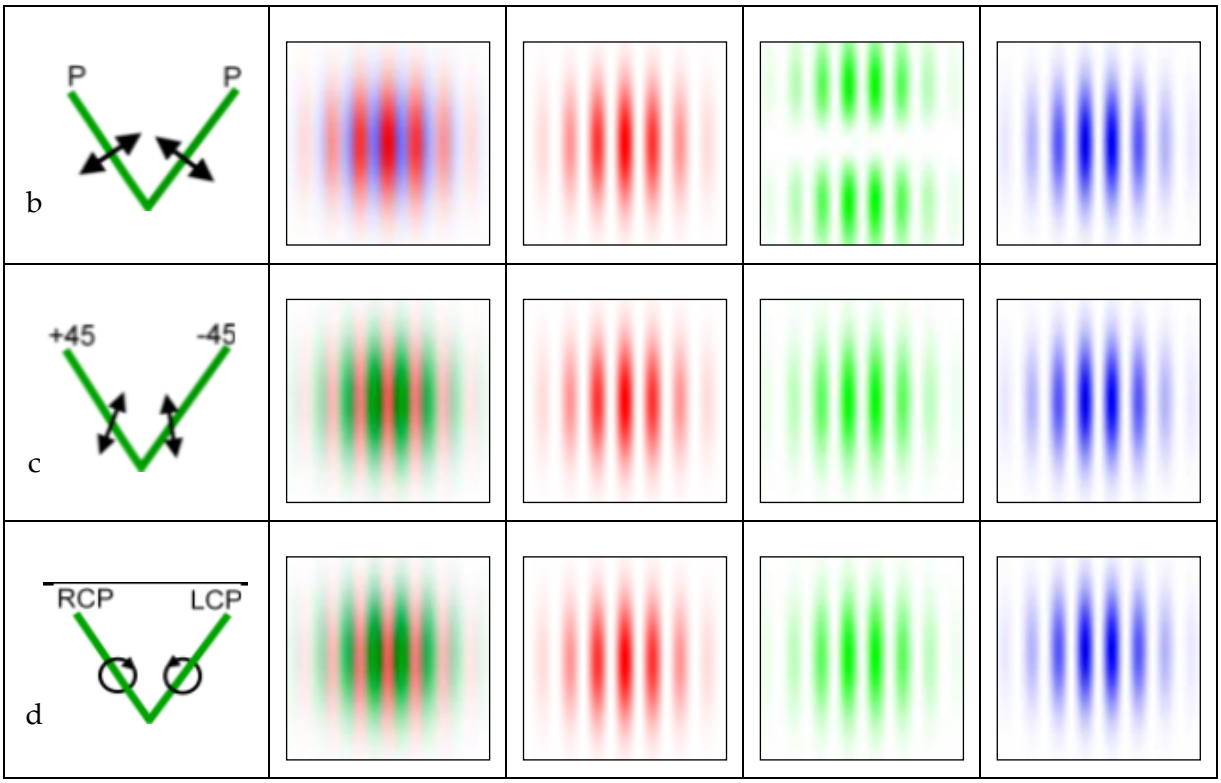

Figure 1. Results of interference of two shifted differently polarized Gaussian beams: (**a**) linear S-polarization; (**b**) linear P-polarization; (**c**) linear polarization at incidence angles of +45° and −45°; (**d**) circular right- and left-handed polarizations (focused electric field components: $|E_x|^2$—red; $|E_y|^2$ —green; and $|E_z|^2$ —blue).

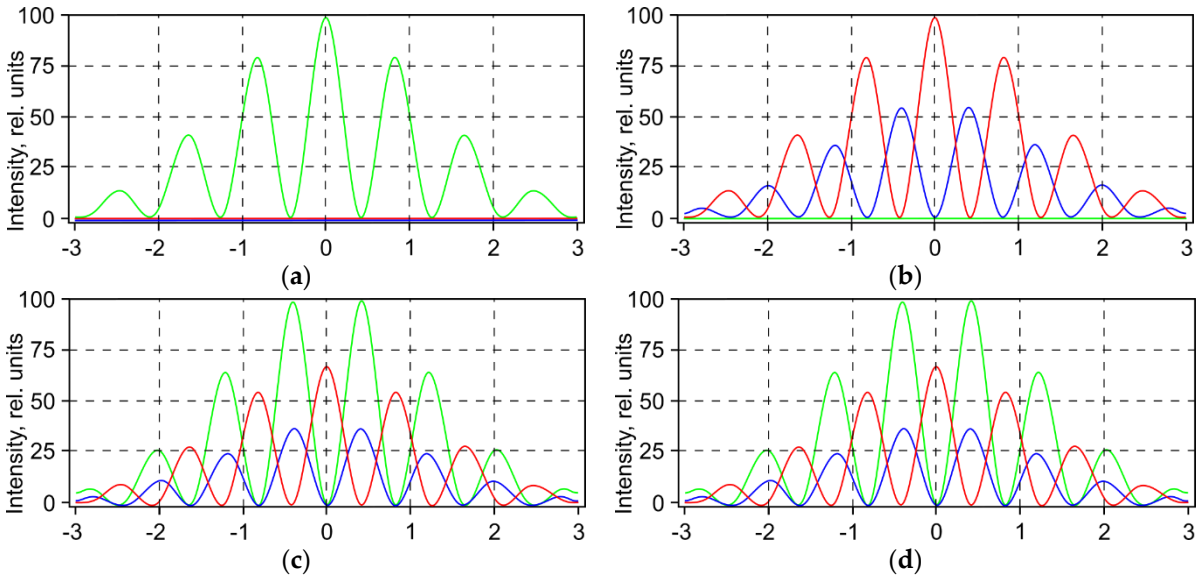

Figure 2. Intensity cross sections of the corresponding focused field components upon interference of differently polarized beams: (**a**) linear S-polarization; (**b**) linear P-polarization; (**c**) linear polarization at incidence angles of +45° and −45°; (**d**) circular right- and left-handed polarizations (focused electric field components: $|E_x|^2$—red; $|E_y|^2$ —green; and $|E_z|^2$ —blue).

With S-polarization (Figures 1a and 2a), the Y-component makes the main contribution to the total intensity distribution, whereas the remaining components are virtually absent.

In the case of P-polarization, the Y-component is virtually absent (Figures 1b and 2b), and the X- and Z-components form shifted gratings. The Z-component here has a maximum energy of all the scenarios in question (Figure 2). According to [37], S- and P-polarizations result in the same deformations of the surface, but with different profile heights. Therefore, we can conclude that the contribution of the Z-component in the case of P-polarization leads to a decrease in the holographic writing efficiency.

Writing with polarized beams at incidence angles of +45° and −45°, as already mentioned, results in the highest relief height. This scenario is well illustrated by the spatial coincidence of the intensity maxima for the Y- and Z-components (Figures 1c and 2c).

For circularly polarized beams, the intensity distribution for the components is identical to the previous case. However, the diffraction efficiency being lower than that for S-polarized beams [37]. This feature can be explained by the fact that in the first case the Y- and Z-components are real (Figure 3a, both green and blue solid lines), and in the second case the Y-component is imaginary (Figure 3b, the green dotted line), which corresponds to the phase difference of the Y- and Z-components equal to 90°.

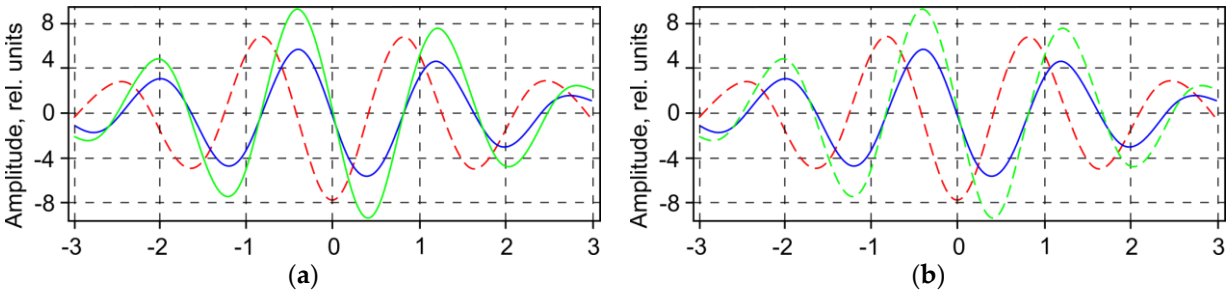

Figure 3. The amplitude functions of the real (solid line) and imaginary (dashed line) parts of the components: (**a**) linear polarization at incidence angles of +45° and −45°; (**b**) circular right- and left-handed polarizations (focused electric field components: X—red; Y—green; and Z—blue).

The analysis shows that the Z-component has a dramatic effect on the formation of linear diffraction gratings on the surface of a multilayer structure based on chalcogenide glass semiconductors As_2S_3 and a-Se. Coincidence or displacement of the grating for the longitudinal component with respect to the grating in other components determines the height of the reliefs formed on the surface of chalcodenides.

On the whole, the above approach makes it possible to obtain a relationship between the distribution of the focused field components and the relief of the produced gratings. Therefore, to study the process of writing forked diffraction gratings, we calculate the components of the electric field upon interference of a Gaussian beam and a first-order vortex beam. A first-order vortex beam with a diameter σ in Cartesian coordinates (x, y) is described by the expression:

$$V(x,y) = \exp\left(-\frac{x^2+y^2}{\sigma^2}\right)(x+iy) \quad (2)$$

In our simulation, we consider a situation when Gaussian and vortex beams are shifted relative to each other along the x axis in the input plane $G\,(x - x_0, y) \pm V\,(x + x_0, y)$. The distributions of the total intensity in the focal plane and the distributions of the intensity of individual electric field components of the studied laser beams were calculated using the Richards–Wolf expressions [41,42]. The calculation results are shown in Figure 4.

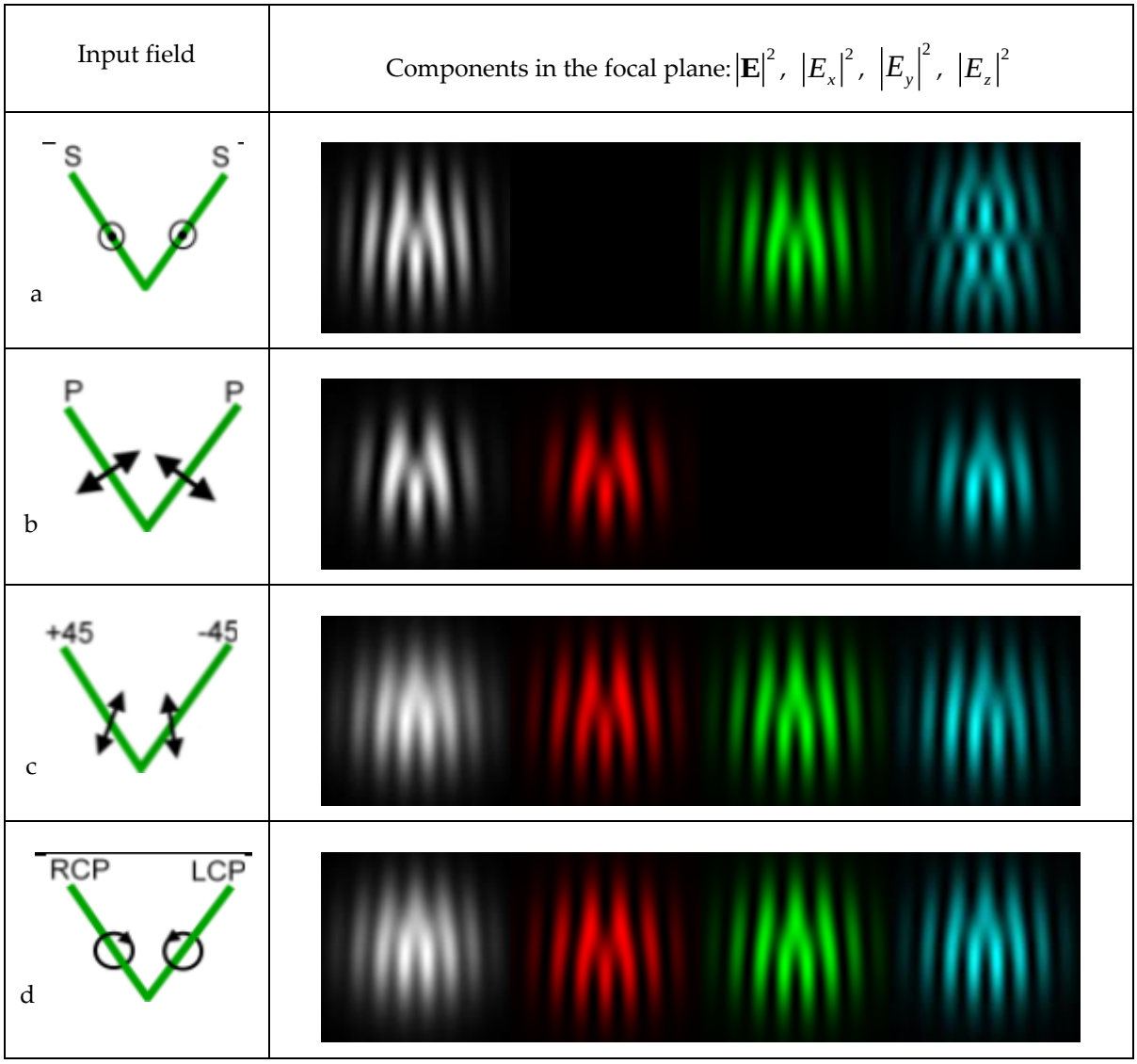

Figure 4. Results of interference of differently polarized Gaussian and first-order vortex beams: (**a**) linear S-polarization; (**b**) linear P-polarization; (**c**) linear polarization at incidence angles of +45° and −45°; (**d**) circular right- and left-handed polarizations (focused electric field components: $|E_x|^2$—red; $|E_y|^2$ —green; and $|E_z|^2$ —blue).

One can see from Figure 4 that the calculated characteristics have significant differences depending on the polarization state of interfering beams. In the case of P- and S-polarizations, the shape of the total intensity of the electric field corresponds to that of the transverse components (Figure 4a,b). Upon interference of beams with orthogonal directions of linear (±45°) and circular polarizations, a spatial coincidence of the intensity distributions of the Y- and Z-components is observed. Moreover, the shape of the total electric field intensity corresponds to their shape (Figure 4c,d).

3. Experimental

As_2S_3 and a-Se chalcogenide glass semiconductors described in this paper have an advantage over azopolymer-based materials [33,34] in the formation of lattice structures. The initial material formed by spraying has high indicators of uniformity of structure and uniformity of thickness. At the same time, the technology of applying multilayer coatings can be carried out by standard industrial technologies for automated application of optical coatings. The use of two types of layers As_2S_3 and a-Se allows optically forming a

microrelief without the use of etching. Moreso, the use of a large number of thin alternating As_2S_3 and a-Se nanolayers makes it possible to increase the degree of heaving of the material with a small response in each pair of layers. This technology is described and studied in detail in earlier works [38]. The optimal parameters of the thickness of the layers were also selected. As in [38], we used a sample of 110 pairs of nanolayers with 9 nm As_2S_3 and 3 nm a-Se with a total thickness of 1.3 microns.

Direct holographic writing of surface forked diffractive structures was performed using a 532-nm, single-mode, linearly polarized laser. A schematic of the experimental setup, which forms the microrelief and records the image of the reflected beam, is shown in Figure 5.

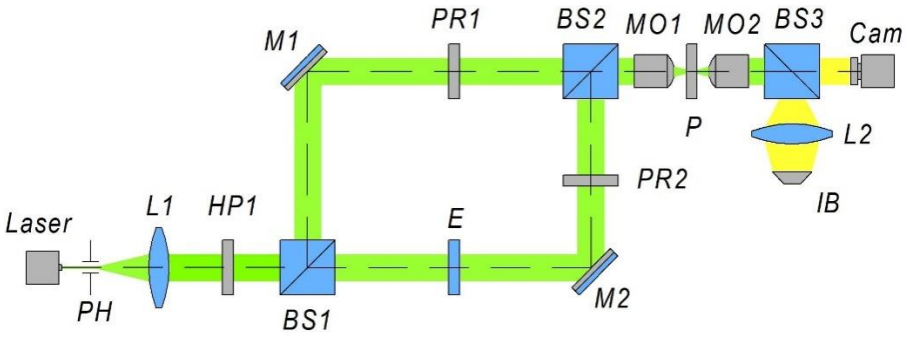

Figure 5. Schematic of the optical setup used in the experiment.

The main element of the setup is a Mach–Zehnder interferometer. The initial linearly polarized Gaussian beam from a solid-state laser was expanded and spatially filtered using a system consisting of a pinhole *PH* (aperture size of 40 μm) and a lens *L1* (focal length of 150 mm). Wave plates *PR1* and *PR2* were used to rotate the initial linear beam polarization in each of the interferometer arms.

The Mach–Zehnder interferometer consists of two mirrors (*M1* and *M2*) and two non-polarizing beam splitters (*BS1* and *BS2*). A spiral phase plate (*E*) was installed in one of the interferometer arms, generating a vortex beam with a topological charge $m = 1$. The non-polarizing beam splitters BS1 and BS2 have a 50:50 shoulder ratio. Losses when using a spiral phase plate are low. The same optical components PS1 and PS2 were used in the interferometer arms, which provides the intensity ratio of the reference, and the vortex beams close to 50:50. A micro-objective *MO1* ($4^{\times}$, NA = 0.1) focused the interfering laser beams from different interferometer arms on the surface of a sample *P*. The duration of the writing time was 3 min, and the power density was 10 W/cm^2. A micro-objective *MO2* ($8^{\times}$, NA = 0.2) and a video camera *CAM* were used to observe the writing process. A system consisting of a lamp *IB*, a spherical lens *L2* (focal length of 50 mm), and a beam splitter *BS3* was used to illuminate the sample surface.

The parameters of the formed gratings were measured using a Solver PRO-M scanning probe microscope (SPM) from the NT-MDT company in the semi-contact regime. According to the measurements, the gratings shown in Figure 4c,d have the highest reliefs. In other cases, microreliefs with a low height comparable to the surface roughness were obtained. SPM images of the formed diffraction gratings are shown in Figure 6a,b.

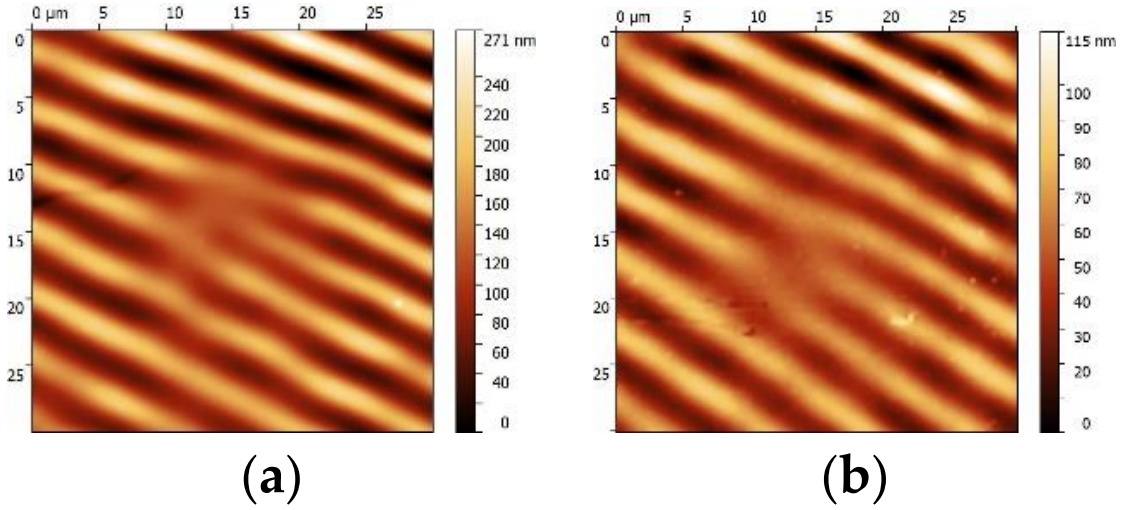

Figure 6. SPM images of the produced structure upon interference of beams with the same polarization: (**a**) linear polarization at incidence angles of +45° and −45°; (**b**) circular right- and left-hand polarizations.

The gratings, as can be seen from Figure 6, have a 'forked' structure. The period of the formed gratings is 5 µm. The height of the lattice formed by interference of beams with linear polarizations of +45° and −45° is 271 nm. The height of the lattice formed by interference of beams with circular polarization of left and right rotation is 115 nm. The height of the profile written with polarized beams at incidence angles of +45° and −45° is two times higher than the profile written with circularly polarized beams. The microreliefs resemble the appearance of the superimposed intensities of the Y- and Z-components, which repeats the result obtained with writing linear gratings. Moreover, some asymmetry is observed, which is characteristic of the distribution of the Z-component for crossed polarization (Figure 4c). A similar effect illustrating the relationship between the longitudinal component of the illuminating beam and the relief of the microstructure formed in a thin film of azopolymers was also observed in [33,34]. Note that this effect is mainly due to the state of polarization of the incident laser light (which may be nonuniform), rather than due to the magnitude of the longitudinal component. The point is that the state of polarization determines nongradient [42,43], or so-called polarization [44–46], optical forces, which most significantly affect the molecules of photosensitive polymers.

4. Results and Discussion

Parameters of vortex beams formed by an element with the highest relief (Figure 6a) were studied using an optical setup in which a collimated laser beam 532 nm was focused by a micro-objective onto the surface of a sample with a fabricated diffraction grating. Using a three-axis translation stage, the diffraction grating was aligned with the beam. The wavelength was the same as that used for holographic writing. The beam intensity was 350 mW/cm^2, and the intensity distribution of the formed vortex beams was recorded by a video camera with a micro-objective. In addition, the topological charge was controlled with a cylindrical lens, which performs astigmatic transformation of the beam.

The intensity distribution of the generated vortex beams before and after passing through the cylindrical lens is shown in Figure 7a,b.

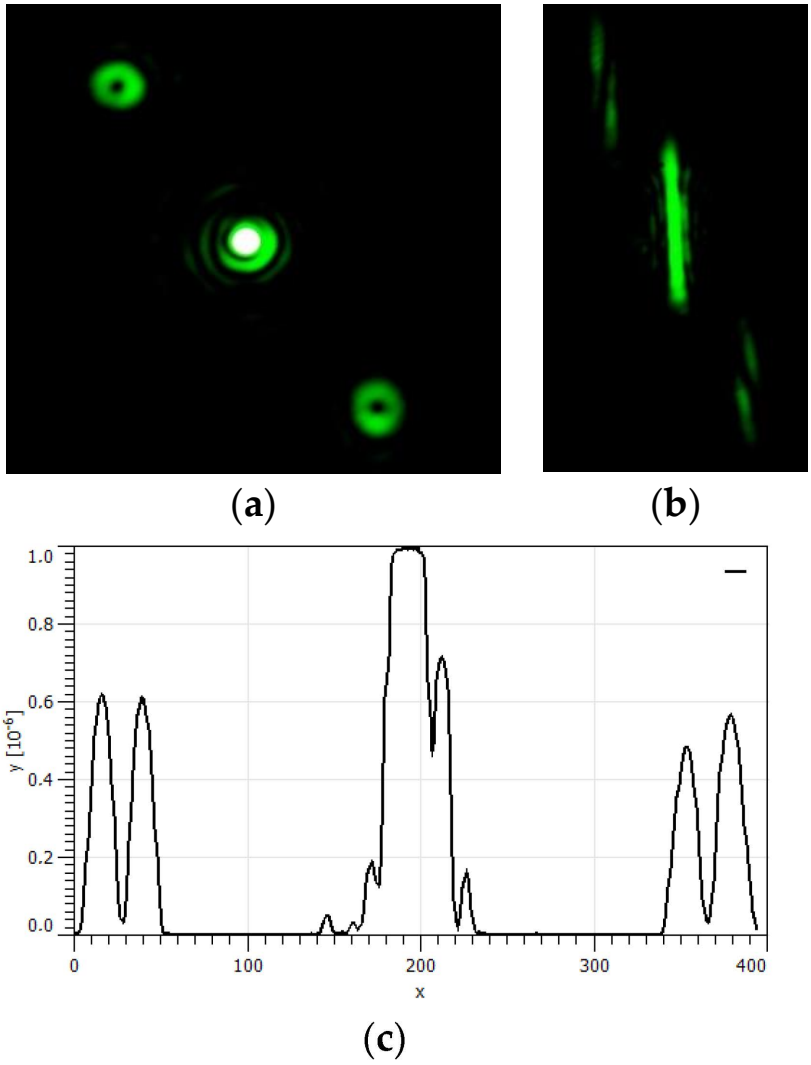

Figure 7. Intensity distributions of vortex beams: (**a**,**b**) before and after passing through a cylindrical lens; (**c**) cross-section profile.

Figure 7a shows that after the beam passes through the diffraction grating, a central beam without a vortex singularity and two off-axis vortex beams are generated. An additional effect of a cylindrical lens allows the astigmatic transformation of the produced beams to be implemented [47–51] in order to visualize the value of the topological charge. Figure 7b shows that the central beam has a zero topological charge, and two off-axis beams have a topological charge equal to unity with different signs ($m = \pm 1$). Note that the diffraction efficiency of the written element is no worse than 37%, which was determined from the intensity profile of the output beams (Figure 7c) by the intensity of the beam of -1 order of diffraction relative to the intensity of the beam of 0 order. However, in the image there is an uneven intensity in the intensity distributions of the vortex beam of +1 and -1 orders of magnitude Figure 7a, which causes an error in determining the diffraction intensity from the image. The actual diffraction efficiency is significantly less.

5. Conclusions

We have presented a method for the formation of forked diffraction gratings in a multilayer structure based on chalcogenide glass semiconductors As_2S_3 and a-Se. The theoretical analysis has shown a strong dependence of the relief height on the longitudinal component of the electric field, with the maximum profile height of the formed gratings

being obtained when the Y- and Z-components coincide. Moreover, this feature is observed both in the formation of linear and forked gratings.

An optical setup based on a Mach–Zehnder interferometer has made it possible to perform holographic writing of diffraction gratings. In this case, a spiral phase plate, which generates a vortex beam with a topological charge $m = 1$,is used to form a vortex phase.

Studies of the parameters of the vortex beams formed by the relief written with crossed polarization have shown that the topological charge of the generated vortex beams is also equal to unity, with the beams in different orders having different signs ($m = \pm 1$). The diffraction efficiency of the written forked grating reaches 37%.

Note in conclusion that the proposed approach can be easily adapted to fabricate other types of DOEs by replacing the phase plate with an element of desired functionality. The numerical and experimental results presented in this study on the formation of lattice structures, as well as fork-shaped structures focused by laser radiation in chalcogenide semiconductor structures, can also be used in areas where high resolution of microrelief formation, high radiation resistance of materials are required; for example, optical memory formation technologies, the formation of optical elements with a metasurface, and plasmon structures [52]. Using focused radiation of different polarizations, it is possible to alternately form different sections of the diffraction element based on lattice elements with different relief features. An example of how the design of the elements took place is described in [53]. Furthermore, research is of applied importance for describing the processes of writing and reading in a polarization-sensitive material [54,55].

Author Contributions: Conceptualization, N.A.I. and S.V.K.; methodology, N.A.I.; software, S.N.K.; validation, N.A.I.; formal analysis S.N.K.; investigation, N.A.I. and V.V.P.; resources, N.A.I. and S.V.K.; data curation, S.V.K.; writing—original draft, N.A.I., V.V.P. and S.N.K.; writing—review and editing, V.V.P., S.V.K. and S.N.K.; visualization, V.V.P.; supervision, S.V.K. and S.N.K.; project administration, N.A.I.; funding acquisition, N.A.I. All authors have read and agreed to the published version of the manuscript.

Funding: This work was funded by the Russian Foundation for Basic Research: 20-52-76021 (realization of direct-laser patterning), as well as by the RF Ministry of Science and Higher Education 007-GZ/CH3363/26 (calculation of electric field components).

Institutional Review Board Statement: Not applicable.

Informed Consent Statement: Not applicable.

Data Availability Statement: Not applicable.

Conflicts of Interest: The authors declare no conflict of interest.

References

1. Shen, Y.; Wang, X.; Xie, Z.; Min, C.; Fu, X.; Liu, Q.; Gong, M.; Yuan, X. Optical vortices 30 years on: OAM manipulation from topological charge to multiple singularities. *Light Sci. Appl.* **2019**, *8*, 90. [CrossRef] [PubMed]
2. Porfirev, A.P.; Kuchmizhak, A.A.; Gurbatov, S.O.; Juodkazis, S.; Khonina, S.N.; Kul'chin, Y.N. Phase singularities and optical vortices in photonics. *Phys. Uspekhi* **2022**, *65*, 789–811. [CrossRef]
3. Chen, J.; Wan, C.; Zhan, Q. Engineering photonic angular momentum with structured light: A review. *Adv. Photonics* **2021**, *3*, 064001. [CrossRef]
4. Willner, A.E.; Huang, H.; Yan, Y.; Ren, Y.; Ahmed, N.; Xie, G.; Bao, C.; Li, L.; Cao, Y.; Zhao, Z.; et al. Optical communications using orbital angular momentum beams. *Adv. Opt. Photonics* **2015**, *7*, 66–106. [CrossRef]
5. Porfirev, A.P.; Kirilenko, M.S.; Khonina, S.N.; Skidanov, R.V.; Soifer, V.A. Study of propagation of vortex beams in aerosol optical medium. *Appl. Opt.* **2017**, *56*, E8–E15. [CrossRef] [PubMed]
6. Khonina, S.N.; Karpeev, S.V.; Paranin, V.D. A technique for simultaneous detection of individual vortex states of Laguerre–Gaussian beams transmitted through an aqueous suspension of microparticles. *Opt. Lasers Eng.* **2018**, *105*, 68–74. [CrossRef]
7. Zhang, L.; Shen, F.; Lan, B.; Tang, A. Mode-dependent crosstalk and detection probability of orbital angular momentum of optical vortex beam through atmospheric turbulence. *J. Opt.* **2020**, *22*, 075607. [CrossRef]
8. Yang, C.; Lan, Y.; Jiang, X.; Long, H.; Hou, J.; Chen, S. Beam-holding property analysis of the perfect optical vortex beam transmitting in atmospheric turbulence. *Opt. Commun.* **2020**, *472*, 125879. [CrossRef]
9. Padgett, M.; Bowman, R. Tweezers with a twist. *Nat. Photonics* **2011**, *5*, 343–348. [CrossRef]

10. Lamperska, W.; Masajada, J.; Drobczyński, V.; Wasylczyk, P. Optical vortex torque measured with optically trapped microbarbells. *Appl. Opt.* **2020**, *59*, 4703–4707. [CrossRef]
11. Bobkova, V.; Stegemann, J.; Droop, R.; Otte, E.; Denz, C. Optical grinder: Sorting of trapped particles by orbital angular momentum. *Opt. Express* **2021**, *29*, 12967–12975. [CrossRef]
12. Skidanov, R.V.; Khonina, S.N.; Kotlyar, V.V. Optical micromanipulation using a binary dynamic light modulator. *Comput. Opt.* **2008**, *32*, 361–365.
13. Forbes, A.; Dudley, A.; McLaren, M. Creation and detection of optical modes with spatial light modulators. *Adv. Opt. Photonics* **2016**, *8*, 200–227. [CrossRef]
14. Khonina, S.N.; Karpeev, S.V.; Butt, M.A. Spatial-light-modulator-based multichannel data transmission by vortex beams of various orders. *Sensors* **2021**, *21*, 2988. [CrossRef] [PubMed]
15. Fadeyeva, T.A.; Shvedov, V.G.; Izdebskaya, Y.V.; Volyar, A.V.; Brasselet, E.; Neshev, D.N.; Desyatnikov, A.S.; Krolikowski, W.; Kivshar, Y.S. Spatially engineered polarization states and optical vortices in uniaxial crystals. *Opt. Express* **2010**, *18*, 10848–10863. [CrossRef]
16. Khonina, S.N.; Morozov, A.A.; Karpeev, S.V. Effective transformation of a zero-order Bessel beam into a second-order vortex beam using a uniaxial crystal. *Laser Phys.* **2014**, *24*, 056101. [CrossRef]
17. Khonina, S.N.; Porfirev, A.P.; Kazanskiy, N.L. Variable transformation of singular cylindrical vector beams using anisotropic crystal. *Sci. Rep.* **2020**, *10*, 5590. [CrossRef]
18. Piłka, J.; Kwaśny, M.; Filipkowski, A.; Buczyński, R.; Karpierz, M.A.; Laudyn, U.A. A Gaussian to Vector Vortex Beam Generator with a Programmable State of Polarization. *Materials* **2022**, *15*, 7794. [CrossRef]
19. Bazhenov, V.Y.; Vasnetsov, M.; Soskin, M. Laser beams with screw dislocations in their wavefronts. *JETP Lett.* **1991**, *52*, 429–431.
20. Khonina, S.N.; Skidanov, R.V.; Kotlyar, V.V.; Soifer, V.A.; Turunen, J. DOE-generated laser beams with given orbital angular moment: Application for micromanipulation. *Proc. SPIE Int. Soc. Opt. Eng.* **2005**, *5962*, 59622W.
21. Moreno, I.; Davis, J.A.; Pascoguin, B.M.L.; Mitry, M.J.; Cottrell, D.M. Vortex sensing diffraction gratings. *Opt. Lett.* **2009**, *34*, 2927. [CrossRef]
22. Stoyanov, L.; Topuzoski, S.; Stefanov, I.; Janicijevic, L.; Dreischuh, A. Farfield diffraction of an optical vortex beam by a fork-shaped grating. *Opt. Commun.* **2015**, *350*, 301. [CrossRef]
23. Kazanskiy, N.L.; Khonina, S.N.; Karpeev, S.V.; Porfirev, A.P. Diffractive optical elements for multiplexing structured laser beams. *Quantum Electron.* **2020**, *50*, 629–635. [CrossRef]
24. Yang, Y.; Ye, X.; Niu, L.; Wang, K.; Yang, Z.; Liu, J. Generating terahertz perfect optical vortex beams by diffractive elements. *Opt. Express* **2020**, *28*, 1417–1425. [CrossRef] [PubMed]
25. Yue, F.; Wen, D.; Xin, J.; Gerardot, B.D.; Li, J.; Chen, X. Vector vortex beam generation with a singleplasmonicmetasurface. *ACS Photonics* **2016**, *3*, 1558. [CrossRef]
26. Degtyarev, S.A.; Volotovsky, S.G.; Khonina, S.N. Sublinearly chirped metalenses for forming abruptly autofocusing cylindrically polarized beams. *J. Opt. Soc. Am. B* **2018**, *35*, 1963–1969. [CrossRef]
27. Zhang, Y.; Liu, W.; Gao, J.; Yang, X. Generating focused 3D perfect vortex beams by plasmonicmetasurfaces. *Adv. Opt. Mater.* **2018**, *6*, 1701228. [CrossRef]
28. Ahmed, H.; Rahim, A.A.; Maab, H.; Ali, M.M.; Mahmood, N.; Naureen, S. Phase engineering with all-dielectric metasurfaces for focused-optical-vortex micro-objective (FOV) beams with high cross-polarization efficiency. *Opt. Mater. Express* **2020**, *10*, 434–448. [CrossRef]
29. Guo, Y.; Zhang, S.; Pu, M.; He, Q.; Jin, J.; Xu, M.; Zhang, X.Y.; Gao, P.; Luo, X. Spin-decoupled metasurface for simultaneous detection of spin and orbitalangular momenta via momentum transformation. *Light-Sci. Appl.* **2021**, *10*, 63. [CrossRef]
30. Ahmed, H.; Rahim, A.A.; Maab, H.; Ali, M.M.; Mahmood, N.; Naureen, S. Highly Efficient PerfectVortex Beams Generation Based on All-Dielectric Metasurface for Ultraviolet Light. *Nanomaterials* **2022**, *12*, 3285. [CrossRef]
31. Fatkhiev, D.M.; Butt, M.A.; Grakhova, E.P.; Kutluyarov, R.V.; Stepanov, I.V.; Kazanskiy, N.L.; Khonina, S.N.; Lyubopytov, V.S.; Sultanov, A.K. Recent advances in generation and detection of orbital angular momentum optical beams—A review. *Sensors* **2021**, *21*, 4988. [CrossRef] [PubMed]
32. Bai, Y.; Lv, H.; Fu, X.; Yang, Y. Vortex beam: Generation and detection of orbital angular momentum. *Chin. Opt. Lett.* **2022**, *20*, 012601. [CrossRef]
33. Porfirev, A.P.; Khonina, S.N.; Khorin, P.A.; Ivliev, N.A. Polarization-sensitive direct laser patterning of azopolymer thin films with vortex beams. *Opt. Lett.* **2022**, *47*, 5080–5083. [CrossRef]
34. Porfirev, A.; Khonina, S.; Ivliev, N.; Meshalkin, A.; Achimova, E. Writing and reading with the longitudinal component of light using carbazole-containing azopolymer thin films. *Sci. Rep.* **2022**, *12*, 1–12. [CrossRef]
35. Cazac, V.; Achimova, E.; Abashkin, V.; Prisacar, A.; Loshmanschii, C.; Meshalkin, A.; Egiazarian, K. Polarization holographic recording of vortex diffractive optical elements on azopolymer thin films and 3D analysis via phase-shifting digital holographic microscopy. *Opt. Express* **2021**, *29*, 9217–9230. [CrossRef] [PubMed]
36. Ivliev, N.A.; Podlipnov, V.V.; Khonina, S.N.; Meshalkin, A.Y.; Akimova, E.A. Single- and Double-Beam Optical Formation of Relief-Phase Diffraction Microstructures in Carbazole-Containing Azopolymer Films. *Opt. Spectrosc.* **2021**, *129*, 489–494. [CrossRef]

37. Achimova, E.; Stronski, A.; Abaskin, V.; Meshalkin, A.; Paiuk, A.; Prisacar, A.; Oleksenko, P.; Triduh, G. Direct surface relief formation on As_2S_3-Se nanomultilayers in dependence on polarization states of recording beams. *Opt. Mater.* **2015**, *47*, 566–572. [CrossRef]
38. Porfirev, A.; Khonina, S.; Meshalkin, A.; Ivliev, N.; Achimova, E.; Abashkin, V.; Prisacar, A.; Podlipnov, V. Two-step maskless fabrication of compound fork-shaped gratings in nanomultilayer structures based on chalcogenide glasses. *Opt. Lett.* **2021**, *46*, 3037–3040. [CrossRef]
39. Abashkin, V.; Achimova, E.; Kryskov Ts Meshalkin, A.; Prisacar, A.; Triduh, G.; Vlcek, M. Investigation of Optical Properties of As2S3–Se Nanomultilayers. In Proceedings of the 2nd International Conference of Nanotechnologies and Biomedical Engineering, Chisinau, Republic of Moldova, 18–20 April 2013; pp. 254–257.
40. Meshalkin, A.; Losmanschii, C.; Prisacar, A.; Achimova, E.; Abashkin, V.; Pogrebnoi, S.; Macaev, F. Carbazole-based azopolymers as media for polarization holographic recording. *Adv. Phys. Res.* **2019**, *1*, 86–98.
41. Richards, B.; Wolf, E. Electromagnetic diffraction in optical systems II. structure of the image field in an aplanatic system. *Proc. R. Soc. Lond. A Math. Phys. Sci.* **1959**, *253*, 358–379.
42. Khonina, S.N.; Ustinov, A.V. Focusing of shifted vortex beams of arbitrary order with differentpolarization. *Opt. Commun.* **2018**, *426*, 359–365. [CrossRef]
43. Wong, V.; Ratner, M.A. Explicit computation of gradient and nongradient contributions to optical forces in the discretedipole approximation. *J. Opt. Soc. A B* **2006**, *23*, 1801–1814. [CrossRef]
44. Wong, V.; Ratner, M.A. Gradient and nongradient contributions to plasmon-enhanced optical forces on silver nanoparticles. *Phys. Rev. B* **2006**, *73*, 075416. [CrossRef]
45. Bian, S.; Williams, J.M.; Kim, D.Y.; Li, L.; Balasubramanian, S.; Kumar, J.; Tripathy, S. Photoinduced surface deformations on azobenzene polymer films. *J. Appl. Phys.* **1999**, *86*, 4498–4508. [CrossRef]
46. Ambrosio, A.; Marrucci, L.; Borbone, F.; Roviello, A.; Maddalena, P. Light-induced spiral mass transport in azo-polymer films under vortex-beam illumination. *Nat. Commun.* **2012**, *3*, 989. [CrossRef]
47. Khonina, S.N.; Ustinov, A.V.; Volotovskiy, S.G.; Ivliev, N.A.; Podlipnov, V.V. Influence of optical forces induced by paraxial vortex Gaussian beams on the formation of a microrelief on carbazole-containing azopolymerfilms. *Appl. Opt.* **2020**, *59*, 9185–9194. [CrossRef]
48. Beijersbergen, M.W.; Allen, L.; Van der Veen HE, L.O.; Woerdman, J.P. Astigmatic laser mode converters and transfer of orbital angular momentum. *Opt. Commun.* **1993**, *96*, 123–132. [CrossRef]
49. Kotlyar, V.V.; Kovalev, A.A.; Porfirev, A.P. Astigmatic transforms of an optical vortex for measurement of its topological charge. *Appl. Opt.* **2017**, *56*, 4095–4104. [CrossRef]
50. Porfirev, A.P.; Khonina, S.N. Astigmatic transformation of optical vortex beams with high-order cylindrical polarization. *J. Opt. Soc. Am. B* **2019**, *36*, 2193–2201. [CrossRef]
51. Khorin, P.A.; Khonina, S.N.; Porfirev, A.P.; Kazanskiy, N.L. Simplifying the experimental detection of the vortex topological charge based on the simultaneous astigmatic transformation of several types and levels in the same focal plane. *Sensors* **2022**, *22*, 7365. [CrossRef]
52. Zhang, Y.; Yang, X.; Gao, J. Generation of polarization singularities with geometric metasurfaces. *Sci. Rep.* **2019**, *9*, 19656. [CrossRef] [PubMed]
53. Zhang, Y.; Yang, X.; Gao, J. Generation of nondiffracting vector beams with ring-shaped plasmonic metasurfaces. *Phys. Rev. Appl.* **2019**, *11*, 064059. [CrossRef]
54. Lin, A.; Wang, J.; Chen, Y.; Qi, P.; Huang, Z.; Tan, X. Reconstruction characters of conventional holography using polarization-sensitive material. *Appl. Opt.* **2022**, *61*, 3134–3140. [CrossRef] [PubMed]
55. Feng, X.; Lu, L.; Yaroshchuk, O.; Bos, P. Closer look at transmissive polarization volume holograms: Geometry, physics, and experimental validation. *Appl. Opt.* **2021**, *60*, 580–592. [CrossRef] [PubMed]